Astron. Astrophys. 353, 363–370 (2000)

ASTRONOMY AND ASTROPHYSICS

CO content of bipolar planetary nebulae

E. Josselin[1], **R. Bachiller**[1], **A. Manchado**[2], **and M.A. Guerrero**[2,3]

[1] Observatorio Astronómico Nacional (OAN), IGN, Apartado 1143, 28800 Alcalá de Henares, Spain
[2] Instituto de Astrofísica de Canarias (IAC), 38200 La Laguna, Tenerife, Spain
[3] Department of Astronomy, University of Illinois, 1002 West Green Street, Urbana, IL 61801, USA

Received 6 August 1999 / Accepted 26 October 1999

Abstract. We report high-sensitivity millimeter-wave CO observations of recently discovered bipolar planetary nebulae (PNe). Three objects (BV 5-1, K 3-94 and K 3-24) have been detected, and one of them (BV 5-1) is resolved by the $\sim 10''$ telescope beam. The envelopes of the three newly detected objects display values of the molecular to ionized mass ratio of ~ 0.2, and sizes of ~ 0.1 pc. This indicates that these PNe are rather evolved, with K 3-24 being the youngest of the three ($\sim 10^3$ years) according to its CO line profile and kinematic ages.

In BV 5-1, the molecular gas appears to be distributed in an irregular disk or ring surrounding the central star and perpendicular to the bipolar nebula. This is similar to the situation found in other better studied bipolar PNe (e.g. NGC 2346, M 2-9, KjPn8), and thus seems to be the rule in this class of objects. This suggests a common mechanism for the rings and the bipolar flows that shape the optical nebula.

Key words: ISM: planetary nebulae: general

1. Introduction

Planetary nebulae (PNe) result from the evolution of stars with initial mass $\lesssim 10\,M_\odot$, after the asymptotic giant branch (AGB) phase (see e.g. Habing 1996, for a recent review). The detection of a neutral gas component, remnant of the AGB envelope, is one of the main observational proofs of this evolutionary scenario. Since the first detection of CO in a PN (namely NGC 7027; Mufson et al. 1975), the number of PNe in which molecular gas has been detected has continuously increased, following the improvements of observational techniques at millimeter waves (for CO observations) and in the infrared (for H_2). A first CO survey of PNe was carried out by Huggins & Healy (1989), who detected 19 PNe among 100 searched. Huggins et al. (1996) increased the number of detections to 44. One of the main results from these studies is that CO emitters are mainly massive ($M_{init} \gtrsim 2.4\,M_\odot$) PNe, coming from a young disk stellar population (type I). Most PNe with a significant molecular envelope are bipolar nebulae, as confirmed by the H_2 survey of Kastner et al. (1996), for whom 80% of the detections were done within this morphological class.

Send offprint requests to: E. Josselin (josselin@oan.es)

The origin of bipolarity is a long standing problem in PNe research. It has long been thought that the interaction between a tenuous fast isotropic wind ($\sim 1000\,\mathrm{km\,s^{-1}}$) and the slow ($\sim 10\,\mathrm{km\,s^{-1}}$) dense wind ejected on the AGB could explain the variety of morphological types (Kwok 1982; Balick 1987). However, recent observations have provided increasing evidence about the importance of high velocity collimated outflows or jets emerging during the post-AGB phase (see e.g. Forveille et al. 1998 for the prototypical case KjPn 8, and Miranda et al. 1999). Interaction with a companion, rotation of the central star, and magnetic fields are usually invoked as possible causes of such asymmetrical mass loss, but more detailed observations of bipolar nebulae are clearly needed.

The interest of CO observations in PNe is twofold. First, since CO molecules are easily excited to the lower rotational levels, a quantitative analysis can provide robust estimates of several parameters such as opacity and mass of the molecular envelope. Moreover, CO observations constitute the most powerful tool to determine the structure and kinematics of the molecular envelopes of massive PNe, a key information to study their bipolarity.

After the CO survey of Huggins et al. (1996), the optical catalogue of PNe compiled by Manchado et al. (1996a) increased the number of known bipolar PNe. These newly identified bipolar objects were obvious interesting targets for CO observations, to obtain a view of the molecular gas in massive PNe as exhaustive as possible. We report in this paper CO observations of some of the most interesting objects.

2. Observations

Observations were carried out in October 1996 and September 1997 with the IRAM 30m radiotelescope on Pico Veleta (near Granada, Spain). The search for molecular gas was made simultaneously in the CO(1-0) and CO(2-1) lines. We used SIS receivers at 3 and 1 mm with single sideband noise temperatures of 80 and 130 K, and typical system temperatures of 400 and 700 K, respectively. The half-power beam width is $22''$ and $10''$ at 3 and 1 mm respectively. The spectrometers were 512×1 MHz filter banks providing a velocity resolution of 2.6 and 1.3 $\mathrm{km\,s^{-1}}$ at 3 and 1mm respectively. The observations were done by wobbling the secondary mirror to a distance of $4'$ from the source.

Table 1. Sample of PNe observed at IRAM. The distances and velocities are taken from Acker et al. (1992) and the optical sizes from Manchado et al. (1996a). The distance is the average of all determinations when different values were given in Acker et al. catalogue. The last three columns indicate the IRAS fluxes at 12, 25 and 60 μm, respectively, where ":" denotes an uncertain flux and L an upper limit (none of the objects in our sample was detected at 100 μm).

Name	PN G	α (J2000.0)	δ (J2000.0)	size ($''$)	distance (kpc)	V_{lsr} (km s^{-1})	S_{12} (Jy)	S_{25} (Jy)	S_{60} (Jy)
M 1-57	022.1–02.4	18 40 20.2	–10 39 47	24.3×10.2	2.76	107	1.27	13.13	16.04:
WeSb 4	031.9–00.3	18 50 40.2	–01 03 14	77×18	.	.			
Sh 2-71	035.9–01.1	19 01 00.1	+02 09 23	200×110	0.74	42	1.41	2.26	4.50
K 3-24	048.7+02.3	19 12 05.8	+15 09 04	12.4×5.8	4.90	.	0.46L	0.37	1.57
M 1-91[a]	061.3+03.6	19 32 57.6	+26 52 44	45×4.6	7.40	.	3.85	8.29	12.14
M 2-48	062.4–00.2	19 50 28.1	+25 54 22	43.6×5.7	4.00	.	1.03L	0.76	7.42
RX J2117.1+3412	080.3–10.4	21 17 07.6	+34 12 22	.	.	.			
BV 5-1[b]	119.3+00.3	00 19 59.3	+62 59 00	75×56[c]	2.19	–64	0.67L	0.28	1.70L
K 3-94	142.1+03.4	03 36 07.9	+60 03 47	20.2×6.8	6.51	.	0.25L	0.26	0.92

[a] M 1-91 is also known as He 2-437 = M 4-15.
[b] BV 5-1 is sometines listed as BV 1 or BV-1.
[c] The size given in Manchado et al. (1996a) corresponds to the bright part of the nebula.

The pointing accuracy, checked every hour, was within 3$''$. Calibration was achieved with a chopper wheel. The intensities given hereafter are in units of main beam brightness temperature.

3. Results

The source sample is presented in Table 1, with data from the Strasbourg-ESO catalog (Acker et al. 1992). We decided to include RX J2117.1+3412 in the sample, since this is one of the widest bipolar PNe known up to now (Appleton et al. 1993). According to their optical sizes, at least three additional objects in our sample (BV 5-1, WeSb 4 and Sh 2-71) could be resolved by the IRAM 30m telescope at λ1.3 mm, since the molecular component, if present, is expected to be equally or more extended than the atomic/ionized one.

3.1. Non-detections

Non-detections are presented in Table 2. Most of these objects suffer from strong interstellar contamination, because of their relative closeness to the galactic plane (height $\lesssim$ 150 pc). M 1-57 displays a two-peak spectrum centered at V_{LSR} = 20 km s^{-1}, with a separation of about 40 km s^{-1}. The discrepancy with the velocity measured in the optical, and the low (2–1)/(1–0) line ratio both indicate that the CO emission is of interstellar origin. Sh 2-71 also displays a two-peak spectrum, centered at the optical nebular velocity. However the occurrence of strong absorption in the same velocity range, the shape and narrowness of the lines ($\Delta V \lesssim 4$ km s^{-1}), the lack of emission at intermediate velocities and the low (2–1)/(1–0) line ratio altogether suggest an interstellar origin. In the case of RX J2117.1+3412, CO emission has been searched without success along a 6$'$-long strip, oriented NW–SE. M 2-48 and M 1-91 were previously searched for H_2 emission but not detected by Kastner et al. (1996). However Guerrero et al. (2000) detected faint H_2 emission in the lobes of M 1-91. Our observations confirm that molecular material is almost absent in these PNe.

Table 2. Limits of the CO non-detections. The rms values (in K) were measured out of interstellar contamination region. The last column indicates the velocity range with strong interstellar contamination.

Name	CO (1–0)	CO (2–1)	IS emission range (km s^{-1})
M 1-57	0.03	0.07	0 to 40
Sh 2-71	0.04	0.11	0 to 55
WeSb 4	0.02	0.04	0 to 115
M 1-91	0.03	0.09	
M 2-48	0.03	0.09	–10 to 40
RX J2117.1+3412	0.01	0.04	

Table 3. Characteristics of the CO detections. The values correspond to the central position.

Name	CO line	V_{lsr} (km s^{-1})	V_{exp} (km s^{-1})	I (K km s^{-1})	T_{mb} (K)	rms (K)
BV 5-1	(1–0)	–74	11	1.1	0.16	0.04
	(2–1)	–73	10	9.7	1.22	0.15
K 3-94	(1–0)	–71	12	1.9	0.15	0.04
	(2–1)	–69	16	14.1	1.04	0.11
K 3-24	(1–0)	47	24	3.0	0.12	0.03
	(2–1)	44	24	23.2	0.88	0.09

3.2. Detections

Three objects have been unambiguously detected in both CO(1–0) and CO(2–1) lines. These are BV 5-1, K 3-94 and K 3-24. All have been mapped, but only BV 5-1 has been clearly resolved. The spectra obtained toward the central position are shown in Fig. 1 and the observational parameters are summarized in Table 3. These three objects are now presented in detail.

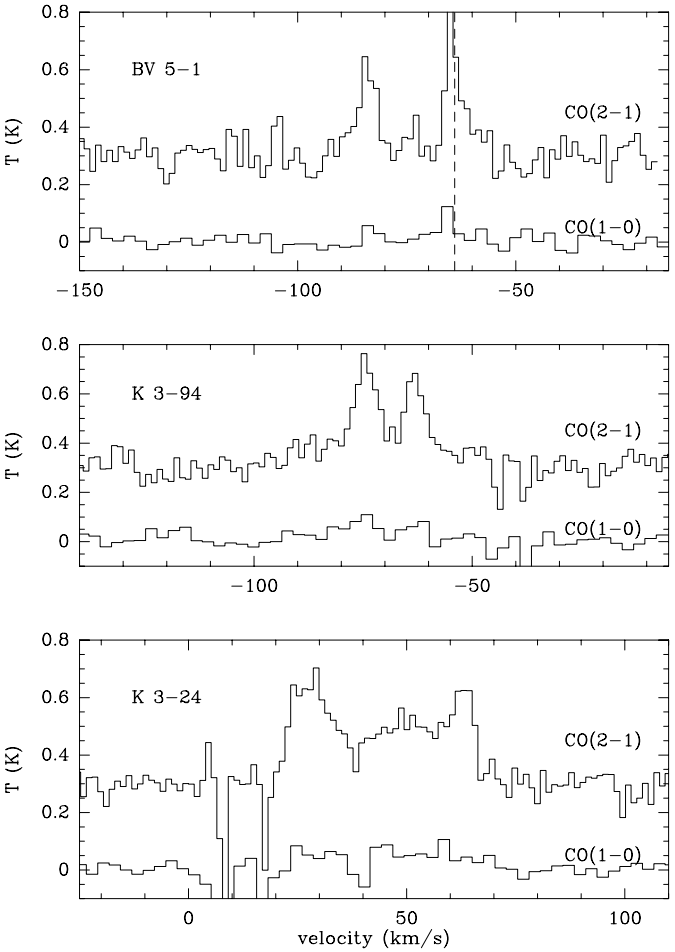

Fig. 1. Spectra of the CO detections. The CO(2–1) lines are shifted by 0.3 K. The dotted line in the upper panel corresponds to the optical radial velocity (no such measurements are available for K 3-94 and K 3-24).

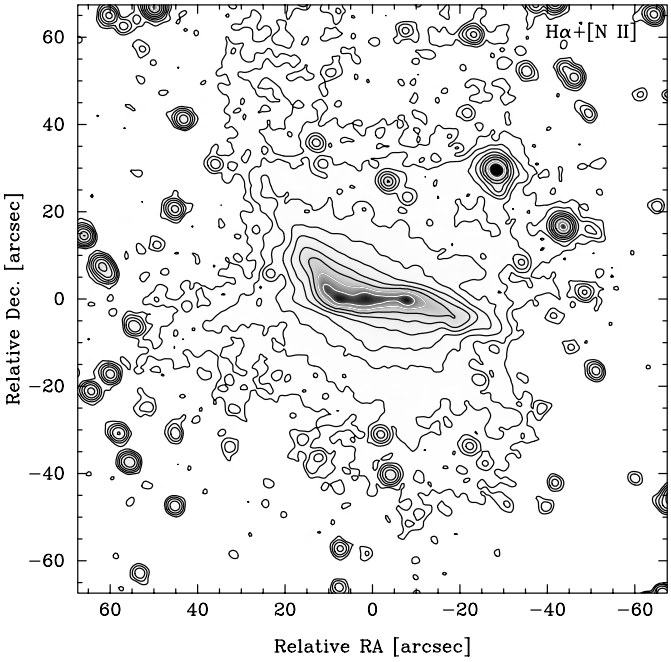

Fig. 2. View of BV 5-1 as seen in an H_α+[N II] filter. Low-level (10% of maximum) contours have been drawn to emphasize the bipolar shape of the nebula.

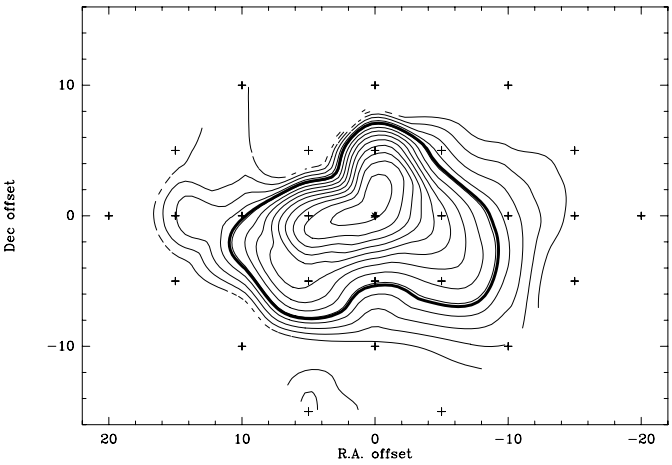

Fig. 3. Contour map of the integrated CO J=2–1 emission from BV 5-1 over the whole velocity range of emission. The contour levels range from 2.2 to 15.4 K km s^{-1}, by steps of 0.55 K km s^{-1}. The heavy contour corresponds to emission at half maximum. The filled star indicates the central position.

3.3. BV 5-1

BV 5-1 is a highly enriched type I PN (N/O=1.5, He/H=0.17; Kaler et al. 1988) with a faint bipolar structure only revealed by deep optical images (Kaler et al. 1988; Manchado et al. 1996a). The nebular symmetry axis, at a position angle on the sky of 162° (see Fig. 2), lies save almost perpendicular to the line of sight. A bright equatorial waist which lies perpendicular to this dominates the morphology of the optical images. This region is highly reddened, and a dark dust lane can be seen at short wavelengths. Kaler et al. (1988) measured expansion velocities in the [N II] line of 11 km s^{-1} along the equatorial axis and 45 km s^{-1} in the bipolar lobes and thus classified it as a middle-to-late butterfly PN. Guerrero et al. (2000) detected H_2 emission along the equatorial waist.

The CO(2–1) and (1–0) spectra displayed in Fig. 1 show two components, the redder one being stronger. The emission ranges from about –90 km s^{-1} to about –55 km s^{-1}, and it is centered near V_{LSR} = –73 km s^{-1}. This is in reasonable agreement with the published optical velocity, regarding the uncertainties of optical measurements (–63.8 km s^{-1}, Acker et al. 1992; see Schneider et al. 1983 for more details). Since millimeter-wave observations generally have a better spectral resolution than optical ones, we think that our determination of the systemic radial velocity is the most accurate so far. The peak-to-peak separation in the CO(2–1) spectrum is 20 km s^{-1}, giving an expansion velocity in excellent agreement with the value measured along the equatorial axis from the low-ionization [N II] line (Kaler et al. 1988). It is worth recalling here that optical measurements of expansion velocities are more precise than those of radial velocities, as the first ones are differential measurements.

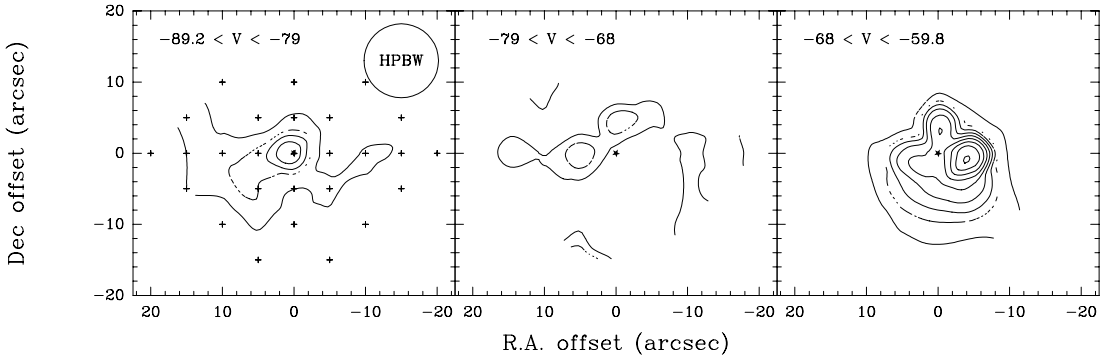

Fig. 4. Contour map of the integrated CO J=2–1 emission from BV 5-1, in the three velocity components (see text). In the first panel, the small crosses indicate the observed positions and the circle shows the IRAM beam (HPBW). In each panel, the central position is indicated by a filled star. The first contour level is 0.65 K km s^{-1} and the step is 0.25 K km s^{-1}.

BV 5-1 is spatially resolved by the CO(2–1) telescope beam. Fig. 3 displays the map of the integrated emission. The nebula appears elongated along an axis approximately E–W, corresponding to the bright component in optical images, shown in Fig. 2. An extension in the northern direction is also seen, which reveals the presence of some molecular material in the brightest part of the bipolar component. The deconvolved extension, measured at half maximum, is 17″, similar to the size of the bright waist observed in the optical. The extension of the CO emitting region, together with its emission velocity range (similar to the optical one) and the high (2–1)/(1–0) line ratio, leave no doubt that the CO emission arises from BV 5-1 with no contamination from intervening interstellar material.

In order to study the kinematic structure of the nebula, it seems natural to divide the CO spectra into three velocity intervals, corresponding to the blue and red shifted components and to the central "gap". The corresponding maps, shown in Fig. 4, are very suggestive of an irregular ring- or torus-like expanding structure. The blueshifted component (left panel of Fig. 4) corresponds to the front (approaching) part of this structure, whereas the redshifted component (right panel of Fig. 4) traces the rear (receding) part. Only weak emission is observed in the central velocity range near the map edges (central panel in Fig. 4). Note that this structure seems to be very clumpy: the blueshifted part is dominated by a clump close to the star position, whereas the redshifted portion has a strong peak 5″ West from the star, and a second one 5″ North.

:381

The velocity structure can be further investigated with the velocity-position diagram (at declination offset 0) shown in Fig. 5. In this diagram the two velocity components are also well seen, and the emission at intermediate velocities is observed to be very weak, and only present at both sides of the star, as corresponds to an expanding ring or torus. An ellipse which shows the expected shape of a velocity-position diagram for a ring-like structure (with parameters derived from the CO(2–1) spectrum and assuming the disk is seen edge-on) is drawn in Fig. 5. Again, the structure is not smooth, but strongly irregular, which confirms the idea that the ring is very disrupted. Unfortunately, the angular resolution of the present observations is too low (with respect to the size of the molecular envelope) to allow a reliable estimate of the ring inclination to the line of sight.

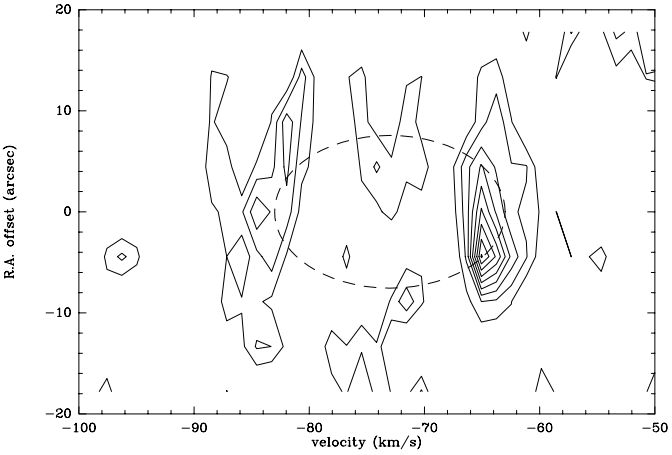

Fig. 5. Velocity-position diagram for BV 5-1 in the CO(2–1) line obtained from a cut at declination offset = 0. The ellipse (dashed line) shows the expected shape for a ring-like structure seen edge-on with an expansion velocity of 10 km s^{-1} and a (not deconvolved) size of 20″.

3.4. K 3-94

On the finding chart shown by Acker et al. (1992), K 3-94 appears quite spherical. However, the narrow-band images obtained by Manchado et al. (1996) reveal a conspicuous bipolar structure composed of a bright elliptical (12″ × 10″) ring and two fainter lobes oriented North–West/South–East. The southern lobe, which is extremely faint and only barely visible on the [N II] image, extends up to 10″ from the center of the ring. The expansion velocity of the central ring, measured in the [N II] and [O III] lines, is 10 km s^{-1} (Sabbadin, Bianchini, and Strafella 1986). The position angle of the central ring, measured by Corradi et al. (1998), is 139°.

The CO spectra of K 3-94 (Fig. 1) also reveal again a double peaked spectrum, the two peaks being at rather same level. The peak-to-peak separation is 12 km s^{-1}, but, as for BV 5-1, emis-

sion extends over a wider range (about 32 km s^{-1}). The radial velocity is V_{LSR} = –70 km s^{-1}.

Emission has been searched around the central position (a 7″ grid in right ascension and declination) but nothing was detected. Therefore the emission is well concentrated in K 3-94, which confirms its nebular (not interstellar) origin. This PN remains thus unresolved by the present observations.

3.5. K 3-24

K 3-24 is one of the quadrupolar PNe identified by Manchado et al. (1996b). They observed two pairs of almost identical lobes, measuring 12″ and 11″, at position angles –20° and 100° respectively, rotated with respect to one another by about 60° on the plane of the sky. The CO(2–1) spectrum shows a complex profile, more flattened than in the cases of BV 5-1 and K 3-94. Interstellar absorption affects probably only the blue edge of the profile, so it is not expected to distort the intrinsic nebular profile. Emission can be seen over a velocity range of 48 km s^{-1}, centered at V_{LSR} = 45 km s^{-1}. Emission as been searched as far as 10″ from the central position. Here again the nebula is not resolved.

The CO line profile is relatively flat, with rather strong emission at the central systemic velocity. This is very different from the CO line profiles observed toward K 3-94 and BV 5-1, in which the central emission gaps are considerably deeper. Mere resolution effects cannot explain the observed differences in the profiles, since K 3-24 lies at a distance which is intermediate between K 3-94 and BV 5-1 (if not closer than both of them; see kinematic distances hereafter). The CO line profile of K 3-24 is typical of very young objects and proto-PNe, and indicates that molecular gas is still present very close to the star. Thus, photodissociation by stellar radiation seems less important in K 3-24 than in the cases of BV 5-1 and K 3-94, which could mean that K 3-24 is younger (so the photodissociation of the molecular envelope has proceeded for a period of time shorter than in the other cases) or that the central star is cooler (see also the kinematic age hereafter).

4. Properties of the molecular envelopes

4.1. Masses of the nebulae

The CO data reported here provide valuable information about the excitation, column densities, and mass of the molecular envelopes. Some relevant physical parameters were derived and are presented in Table 4. They are discussed hereafter.

CO column densities can be estimated for optically thin CO(2–1) emission under LTE conditions from the standard expression

$$N(CO) = 1.06 \times 10^{13} T_{ex} \exp(16.5/T_{ex}) \int T_R(2-1) dv \quad (1)$$

where T_{ex} is the excitation temperature and T_R is defined by Kutner and Ulrich (1981) (see e.g. Bachiller et al. 1989a and 1993). The value of T_{ex} can in principle be estimated from the CO (2–1)/(1–0) intensity ratio. In the particular case of the small

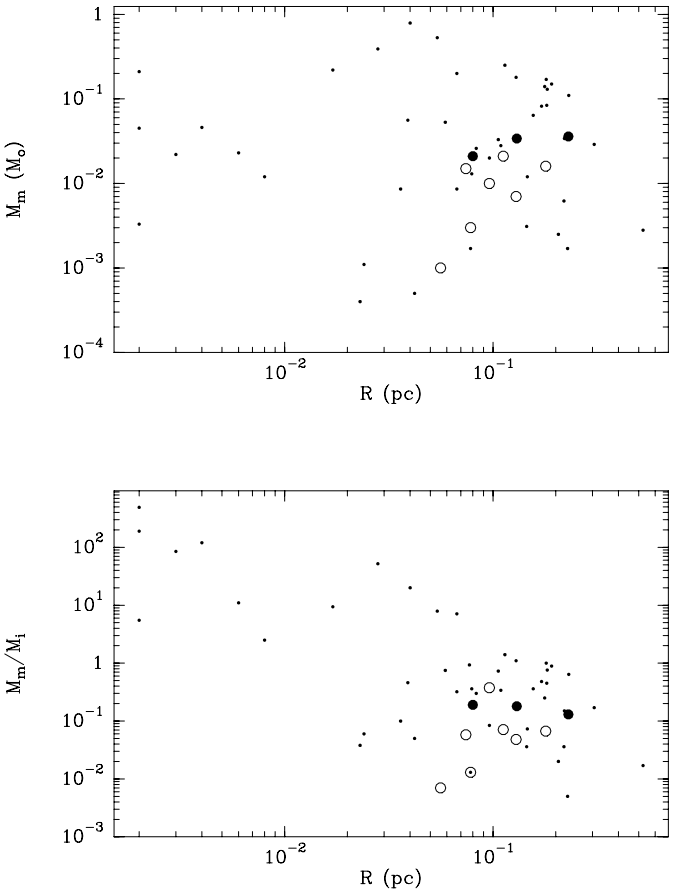

Fig. 6. Check of the evolutionary status of the objects from our sample. Filled circles correspond to CO detections. Empty circles correspond to CO non-detections and thus denote upper limits of M_m and M_m/M_i. Small dots coorespond to data from Huggins et al. (1996).

PNe discussed here, beam dilution is very important making difficult the estimate of the *intrinsic* intensity ratio (i.e. the ratio corrected for all instrumental effects). The intrinsic (2–1)/(1–0) intensity ratio cannot exceed a value of 4, which corresponds to the limit in the totally optically thin case. If the nebulae were point-like sources, the *observed* intensity ratio would be at most $\sim$ 19, i.e. the intrinsic ratio multiplied by the square of the beam ratio. In the case of the three PNe detected in both CO lines, the observed values of intensity ratio are about 8, but CO emission may fill at least the 1mm beam. So we conclude that the intrinsic values of the ratio are probably quite high (close to 4), indicating both optically thin CO emission and rather high excitation temperatures.

We have used the approximation of the above formula given by Huggins et al. (1996):

$$N(CO) = 1 \times 10^{15} I_{CO(2-1)}\ cm^{-2} \quad (2)$$

which is exact for T_{ex} = 7 and 77 K and reliable within a factor of 2 for T_{ex} = 5–150 K. The values found for the column densities are typically about 10^{16} cm^{-2} (see Table 4). The total gas column densities can be derived from the CO column densities: N(H) = N(CO)/f, where f is the value of the CO/H abundance

Table 4. Properties of detected PNe. D_K stands for kinematic distance (see text).

Name	D_K (kpc)	CO size	age (10^3 yrs)	N(CO) (10^{15} cm^{-2})	M_m ($10^{-2}M_\odot$)	M_m/M_i	$(\dot{M}v_{exp})/(L_\star/c)$
BV 5-1	5.5	17″	10.7	6.1	3.6	0.13	9.1[a]
K 3-94	5.5	$\lesssim$10″	$\lesssim$2.9	16.3	$\sim$3.4	$\sim$0.18	$\sim$9.1[b]
K 3-24	3.5	$\lesssim$10″	$\lesssim$1.1	25.0	$\sim$2.1	$\sim$0.19	$\sim$22.7[b]

[a] with $L_\star$ = 200 $L_\odot$ (cf. Kaler et al. 1988)
[b] with $L_\star$ = 1000 $L_\odot$ (assumed, as no data are available.)

ratio. We will assume solar abundance for C and that all carbon is in the form of CO, i.e. f $\sim$ 3 10^{-4}; this may lead to an under-estimation of N(H), as part of C may be in the form of atomic and/or singly-ionized form, but but such proportion is unknown.

The mass of the molecular component, assuming that most H is in form of H_2, is given by:

$$M_m \;=\; 2.6 \times 10^{-10} F D^2 / f \; M_\odot \qquad (3)$$

where F is the CO line flux in K km s^{-1} sq. arsecs and the distance D is in kpc (see e.g. Huggins et al. 1996). A good knowlege of the distance is thus a key point in this determination. Distances given in Acker et al. (1992) are statistical distances, which assume the same mass of ionized gas for all PNe. This does not apply to bipolar PNe, among the most massive PNe. We then used kinematical distances (a more reliable measurement for such low latitude objects) derived from the calculated radial velocities, and following the rotation curve of Burton (1974). These distances are listed in Table 4. The distance for BV 5-1 is remarkably larger than the one listed by Acker et al. (1992), showing that its ionized mass is indeed much greater than the average one assumed for all PNe.

The ratio between the mass of the molecular component and the mass of the ionized component, M_m/M_i, should be a good indicator of the evolutionary stage of a PN, since the ionized nebula grows at the expense of the molecular nebula, so the M_m/M_i ratio is expected to decrease as the PN evolves.

The mass of the ionized component can be derived from the λ 6 cm emission (see e.g. Gathier 1987):

$$M_i \;=\; 8.85 \times 10^{-9} n_e D^3 \theta^3 \frac{1+4y}{1+y+xy} \qquad (4)$$

where D is the distance in kpc, θ the size in arcsec, y the helium abundance, x the fraction of doubly ionized helium, and the electron density n_e is given by

$$n_e \;=\; 5.73 \times 10^2 S_{5GHz}^{1/2} T_e^{1/4} D^{-1/2} \theta^{-1/2} \left(\frac{1+y+3xy}{1+y+xy}\right)^{-1/2} \qquad (5)$$

with S_{5GHz} in mJy and T_e the electron density in K. Values of T_e, x and y have been taken from Cahn et al. (1992) and are reported in Table 5. Values of T_e = 1.02 10^4 K, x = 0.5 and y = 0.11 are assumed when no measurement are available. We obtain that the three PNe with positive CO detections display similar values of M_m/M_i, about 0.2.

Table 5. Relevant parameters for the estimation of the mass of the ionized envelope (see text). WeSb 4 was not included, as neither 5 GHz observations nor estimations of T_e, x and y are available.

Name	S_{5GHz} (mJy)	T_e (10^4 K)	x	y
BV 5-1	<0.5	1.41	0.387	0.170
K 3-94	5.5	1.02	0.500	0.110
M 1-57	69.0	1.02	0.386	0.110
Sh 2-71	66.0	1.42	0.621	0.110
K 3-24	26.0	1.02	0.500	0.110
M 1-91	0.7	1.02	0.500	0.110
M 2-48	19.0	1.02	0.500	0.110

In the case of non-detections, an upper limit to the molecular mass has been estimated, taking the 2σ limit for T_{mb} and 10 km s^{-1} for the expansion velocity. The M_m/M_i ratio is lower, by up to one of magnitude, for these PNe not detected in CO.

4.2. Evolutionary status

The new CO data are particularly relevant with regard to the evolutionary status of the observed sample of PNe. For instance, non-detections should indicate rather evolved objects in which most molecules have already been photodissociated. The central star of the large nebula RX J2117.1+3412 is a white dwarf detected by ROSAT (Motch et al. 1993). The non-detection of CO in this nebula, unaffected by interstellar contamination, confirms that it is a very evolved object. The case of M 1-91 may be more complicated. According to Goodrich (1991), it is similar to M 2-9, usually considered as a young planetary nebula, but could also be a symbiotic star, so that the lack of molecular material could reflect the presence of a hot companion. Unfortunately our data do not provide significantly new information on the evolutionary status of the PNe affected by severe contamination by interstellar CO emission (namely M 1-57, WeSb 4, Sh 2-71 and M 2-48). Other tracer of the molecular component (e.g. CN or HCN) should be searched to make a reliable study of their evolutionary status.

All three objects detected in CO appear rather similar, with comparable M_m/M_i ratio about 0.2 and sizes of the envelopes about 0.1 pc. This suggests similar evolutionary stages, although the CO profile shape of K 3-24 indicates this could be younger than K 3-94 and BV 5-1. Since these objects have not been much studied so far, it seems interesting to look for analogies

with other better studied PNe. Regarding the M_m/M_i ratio and the size of the nebula, BV 5-1 is similar to NGC 6445, a well-known bipolar PN at the same distance from the Sun (2.2 kpc). K 3-94 and K 3-24 may be at some intermediate evolutionary stage between the well-studied bipolar PNe NGC 6772 and NGC 2440. Anyhow these comparisons should not be pushed too far. For example, NGC 6445 is more massive than BV 5-1 (by a factor 2.4) and should then result from a more massive progenitor.

It is also interesting to study how these new detections fit in with the analysis of previous CO surveys works. Fig. 6 shows the molecular mass and the molecular-to-ionized mass vs. nebular radius for our data, and the survey observations of Huggins et al. (1996). Clearly the new data fit well within the survey results. The (M_m/M_i) parameter is probably the most confident indicator of evolution, since it depends on the distance only as $D^{-1/2}$. Thus, the three detected objects appear rather evolved, owing to the relatively low values of the M_m/M_i ratio.

Ages given in Table 4 are kinematic time-scales calculated from the optical sizes divided by the expansion velocities measured on the CO profiles. We note that K 3-24 appears younger than BV 5-1 and K 3-94, as expected from the direct comparison of the CO profiles. This is because the expansion velocity of the K 3-24 molecular envelope is about twice as high as those of BV 5-1 and K 3-94. On the other hand, the similarity in the current values of the M_m/M_i ratios in all three PNe could indicate that K 3-24 is less massive, so the ionized region has grown faster than in the other two nebulae.

Combining the kinematic ages and the masses of the molecular envelopes, we have derived rough AGB mass-loss rates. Part of the mass ejected on the AGB has been ionized, so these estimates are lower limits. The ionized mass may, however, still be dominated by material lost during the post-AGB phase, so that using M_m+M_i as the total mass ejected on the AGB would lead to overestimation of the mass-loss rate during the AGB phase. Such rates can be used to estimate the ratio of the outflow momentum to the radiation momentum (last column in Table 4). We find that $\dot{M}v_{exp} >> L_\star/c$ in all three objects. This may reflect either a drop of the stellar luminosity after the onset of PN formation (if mass loss is driven by radiation pressure on grains) or a binary star interaction, responsible for mass loss (see Bachiller et al. 1989b). If we assume a typical value of 10^4 $L_\odot$ for the luminosity on the AGB, the luminosity of the central star of BV 5-1 has decreased by a factor of about 50, which is roughly the value of the $\dot{M}v_{exp}/(L_\star/c)$ ratio. Then, the drop of the stellar luminosity appears as the most likely explanation. In the case of NGC 2346 studied by Bachiller et al. (1989b), with the same AGB luminosity and 31 $L_\odot$ for the current luminosity of the central stellar system, one finds a decrease by a factor of about 300, while the $\dot{M}v_{exp}/(L_\star/c)$ ratio is about 2000. Nevertheless, the luminosity on the AGB is poorly known, and the hypothesis of mass transfer in a binary system cannot be ruled out.

As shown in Table 1, all the objects of our sample are rather weak far-infrared emitters. The investigation of the dust content based on IRAS data in these PNe is then rather limited. We note however that those objects not detected in CO seem to display lower values of the [25]–[60] colours than detected ones. Such a decrease of this colour is generally interpreted as an increase of the dust temperature. In the case of PNe, this could mean that dust is reheated as the ionized nebula grows. This is again consistent with the evolutionary sequence described above.

4.3. Geometry and dynamics of the envelopes

In BV 5-1 a ring structure has clearly been revealed by the new CO observations. Moreover, the similar two-peaked CO profiles observed toward K 3-94 and K 3-24 suggest a similar geometry for these objects. Concerning K 3-24, the relative flatness of its spectrum makes the hypothesis of a ring cautious, as a spherical shell can produce a quite similar CO profile. Furthermore, as discussed above, if it is a ring, it may be less detached from the central star, i.e, the actual structure could be more similar to a disk. Similar ring- or disk-like molecular envelopes have clearly been detected in the nearby PN NGC 2346 and, thanks to interferometric CO observations, at the waist of the prototypical Butterfly nebula M 2-9 (Zweigle et al. 1997) and at the center of the multipolar nebula KjPn8 (Forveille et al. 1998). In all the cases in which the ring orientation is known, it is found that the ring is perpendicular to the bipolar optical structure (the youngest bipolar jets is in the case of KjPn8). The origin of such rings or disks is still unclear. One possibility is that they result from an accretion disk generated by mass transfer in a binary or multiple system. Indeed BV 5-1 and K 3-94 belong to the cases discussed by Soker (1997), in which the shape of the optical nebulae may result from the interaction with (sub)stellar companion(s), with or without a common envelope phase. Since these rings are relatively thin, it seems unlikely that they are the collimating agents of the flows which generate the bipolar structures. Moreover, in multipolar nebulae (e.g. KjPn8, K 3-24) these rings can coexist with pairs of bipolar flows emerging at very different directions. In the case of K 3-24, Manchado et al. (1996b) suggest that this type of nebulae can be formed by precession of the ejection axis, perhaps due to precession in the rotation axis of the central star. Bipolar flows and equatorial disks could be generated by a common cause, such as the mentioned mass transfer in a multiple system. However, since no companions have been detected up to now for most of these objects, other possible mechanisms (such as those related to stellar rotation and magnetic fields) cannot be ruled out as the final cause of the bipolarity of these objects. Furthermore the clumpy and disrupted structure of the ring of BV 5-1 may reveal instabilities in the disk or a complex mass-loss history (time variations or turbulent processes). Whatever the mechanism involved, our observations confirm that the formation of dense equatorial disks and bipolar flows are basic mechanisms in the formation and shaping of planetary nebulae.

5. Conclusions

We report high-sensitivity CO observations of recently identified bipolar PNe, which complement previous studies, in par-

ticular those of Huggins et al. (1996). In our sample, three new detections were achieved. All three objects seem be at roughly the same evolutionary stage, regarding their molecular to ionized mass ratio. Among them, BV 5-1 is the only one which could be resolved with single-dish observations. The molecular envelope of BV5-1 clearly displays a ring- or torus-like structure. Similar CO spectral profiles for the two other detections (K 3-94 and K 3-24) suggest similar distributions of the circumstellar molecular gas. Nevertheless, the dynamical age and CO(2-1) profiles strongly suggest that K 3-24 is the youngest among the three PNe. These irregular ring or disk-like structures seem to be very common in bipolar PNe. They could result from the same mechanism generating the flows which shape bipolar and multipolar nebulae.

Acknowledgements. We are grateful to P.J. Huggins for helpful comments and suggestions, to M. Pérez Gutiérrez and C. Codella for help with the observations and data reduction and to an anonymous referee for useful comments. This research has made use of the Simbad database, operated at CDS, Strasbourg, France. EJ and RB aknowledge partial support from spanish DGESIC grants PB 96–104 and SB 97–22043. A. M. and M.A.G. aknowledge partial support by Spanish grants PB94-1108 and PB97-1435-C02-01. M.A.G. is also partially supported by the Dirección General de Enseñanza Superior and Investigación Científica of Spanish Ministerio de Educación y Cultura.

References

Acker A., Ochsenbein F., Sternholm B., et al., 1992, Strasbourg-ESO Catalogue of Galactic Planetary Nebulae
Appleton P.N., Kawaler S.D., Eitter J.J., 1993, AJ 106, 1973
Bachiller R., Huggins P.J., Cox P., Forveille T., 1993, A&A 267, 177
Bachiller R., Bujarrabal V., Martín-Pintado J., Gómez-Gonzalez J., 1989a, A&A 218, 252
Bachiller R., Planesas P., Martín-Pintado J., Bujarrabal V., Tafalla M., 1989b, A&A 210, 366
Balick B., 1987, AJ 94, 671
Burton W.B., 1974, In: Verschuur G., Kellermann K.I. (eds.) Galactic and extra-galactic radio astronomy. Springer
Cahn J.H., Kaler J.B., Stanghellini L., 1992, A&AS 94, 399
Corradi R.L.M., Aznar R., Mampaso A., 1998, MNRAS 297, 617
Forveille T., Huggins P.J., Bachiller R., Cox P., 1998, ApJ 495, L111
Gathier R., 1987, A&AS 71, 245
Goodrich R.W., 1991, ApJ 366, 163
Guerrero M.A., Villaver E., Manchado A., García-Lario P., Prada F., 2000, ApJS, in press
Habing H.J., 1996, A&AR 7, 97
Huggins P.J., Healy A.P., 1989, ApJ 3436, 201
Huggins P.J., Bachiller R., Cox P., Forveille T., 1996, A&A 315, 284
Kaler J.B., Chu Y.-H., Jacoby G.H., 1988, AJ 96, 1407
Kastner J.H., Weintraub D.A., Gatley I., Merrill K.M., Probst R.G., 1996, ApJ 462, 777
Kutner M.L., Ulrich B.L., 1981, ApJ 250, 341
Kwok S., 1982, ApJ 258, 280
Manchado A., Guerrero M.A., Stanghellini L., Serra-Ricart M., 1996a, The IAC morphological catalog of northern galactic planetary nebulae
Manchado A., Stanghellini L., Guerrero M.A., 1996b, ApJ 466, L95
Miranda L.F., Vazquez R., Corradi R.L.M., et al., 1999, ApJ, in press
Motch C., Werner K., Paukll M.W., 1993, A&A 268, 561
Mufson S.L., Lyon J., Marionni P.A., 1975, ApJ 201, L85
Sabbadin F., Bianchini A., Strafella F., 1986, A&AS 65, 259
Schneider S.E., Terzian Y., Purgathofer A., Perinotto M., 1983, ApJS 52, 399
Soker N., 1997, ApJS 112, 487
Zweigle J., Neri R., Bachiller R., Bujarrabal V., Grewing M., 1997, A&A 321, 891